



Article

# Directly Anodized Sulfur-Doped TiO<sub>2</sub> Nanotubes as Improved Anodes for Li-ion Batteries

Davood Sabaghi <sup>1,2</sup>, Mahmoud Madian <sup>1,3,\*</sup> , Ahmad Omar <sup>1,\*</sup>, Steffen Oswald <sup>1</sup>, Margitta Uhlemann <sup>1</sup>, Morteza Maghrebi <sup>2</sup>, Majid Baniadam <sup>2</sup>  and Daria Mikhailova <sup>1,\*</sup>

<sup>1</sup> Leibniz Institute for Solid State and Materials Research (IFW) e. V., 01069 Dresden, Germany; davoodsabagh@gmail.com (D.S.); s.oswald@ifw-dresden.de (S.O.); m.uhlemann@ifw-dresden.de (M.U.)

<sup>2</sup> Department of Chemical Engineering, Faculty of Engineering, Ferdowsi University of Mashhad, Mashhad 9177948974, Iran; mmaghrebi@um.ac.ir (M.M.); baniadam@um.ac.ir (M.B.)

<sup>3</sup> National Research Centre, Physical Chemistry Department, 33 El-Buhouth St., Giza 12622, Egypt

\* Correspondence: mmadian2@gmail.com (M.M.); a.omar@ifw-dresden.de (A.O.); d.mikhailova@ifw-dresden.de (D.M.)

Received: 10 July 2020; Accepted: 6 October 2020; Published: 19 October 2020



**Abstract:** TiO<sub>2</sub> represents one of the promising anode materials for lithium ion batteries due to its high thermal and chemical stability, relatively high theoretical specific capacity and low cost. However, the electrochemical performance, particularly for mesoporous TiO<sub>2</sub>, is limited and must be further developed. Elemental doping is a viable route to enhance rate capability and discharge capacity of TiO<sub>2</sub> anodes in Li-ion batteries. Usually, elemental doping requires elevated temperatures, which represents a challenge, particularly for sulfur as a dopant. In this work, S-doped TiO<sub>2</sub> nanotubes were successfully synthesized in situ during the electrochemical anodization of a titanium substrate at room temperature. The electrochemical anodization bath represented an ethylene glycol-based solution containing NH<sub>4</sub>F along with Na<sub>2</sub>S<sub>2</sub>O<sub>5</sub> as the sulfur source. The S-doped TiO<sub>2</sub> anodes demonstrated a higher areal discharge capacity of 95 μAh·cm<sup>-2</sup> at a current rate of 100 μA·cm<sup>-2</sup> after 100 cycles, as compared to the pure TiO<sub>2</sub> nanotubes (60 μAh·cm<sup>-2</sup>). S-TiO<sub>2</sub> also exhibited a significantly improved rate capability up to 2500 μA·cm<sup>-2</sup> as compared to undoped TiO<sub>2</sub>. The improved electrochemical performance, as compared to pure TiO<sub>2</sub> nanotubes, is attributed to a lower impedance in S-doped TiO<sub>2</sub> nanotubes (STNTs). Thus, the direct S-doping during the anodization process is a promising and cost-effective route towards improved TiO<sub>2</sub> anodes for Li-ion batteries.

**Keywords:** doped TiO<sub>2</sub>-nanotubes; in-situ sulfur doping; titanium anodization

## 1. Introduction

In the last decade, with the increasing demand for rechargeable energy storage, significant attention has been paid towards convenient fabrication of next generation electrode materials with both high power and high energy densities [1]. Accordingly, research has been oriented towards nanostructuring of electrodes for high-performance energy storage devices such as supercapacitors and Li-ion batteries (LIBs) [2,3]. In this regard, mesoporous TiO<sub>2</sub> has attracted great attention as a perspective anode for LIBs due to its high stability, low cost, and good rate performance [4,5]. Moreover, the high Li<sup>+</sup> insertion potential above 1.5 V vs. Li can effectively suppress the formation of Li dendrites during cycling, in contrast to metallic Li and graphitic anodes [6]. A variety of TiO<sub>2</sub>-based nanostructures had already been explored for energy storage, such as nanoparticles, microspheres, and nanotubes [7]. Among those, TiO<sub>2</sub> nanotubes have gained the highest importance due to their high surface area and uniform pore size distribution [7,8].

Furthermore, TiO<sub>2</sub> has an advantage of cycling stability due to relatively low volume expansion (less than 1%) during lithium insertion/extraction. In the sense of theoretical capacity, TiO<sub>2</sub> exhibits a capacity of 336 mAh·g<sup>-1</sup>, as assumed for insertion of 1 Li per formula unit, which represents double the theoretical capacity of a well-studied Li<sub>4</sub>Ti<sub>5</sub>O<sub>12</sub> [6]. However, a slower Li<sup>+</sup> diffusivity and relatively poor electronic conductivity for Ti-based oxides particularly impedes high rate performance, leading to lower capacities [9].

To date, several strategies for improvement of the transport of lithium ions and electrons in TiO<sub>2</sub> electrodes such as controlling morphology via nanosizing [10,11], hybridizing with other conductive materials [12,13], and elemental doping of the TiO<sub>2</sub> networks [14,15] have been successfully performed. In particular, doping of TiO<sub>2</sub> with non-metallic elements can remarkably increase the electronic conductivity. For example, doping of crystalline TiO<sub>2</sub> with sulfur [16,17], nitrogen [18], and fluorine [19] significantly enhanced the rate capability, as a result of the improved electronic conductivity of the material. Among the non-metallic dopants, S exhibits a larger ionic radius compared to N and F, which results in narrowing of the band gap in S-doped TiO<sub>2</sub> [20]. Up to now, numerous efforts have been undertaken to synthesize S-doped TiO<sub>2</sub> networks, such as oxidation of TiS<sub>2</sub> using hydrothermal synthesis [21] or a sol-gel method [22]. Li et al. prepared S-doped anatase TiO<sub>2</sub> electrodes through a hydrothermal reaction at 500 °C for 2 h in an Ar-flow. The S-doped anatase TiO<sub>2</sub> could further facilitate the electron and ion pathways during electrochemical cycling [23]. Ni et al. also presented the preparation of S-doped TiO<sub>2</sub> array anodes for sodium storage by sulfidation of TiO<sub>2</sub> nanotubes at a 500 °C with a robust rate capability of 167 mAh·g<sup>-1</sup> at 3.35 Ag<sup>-1</sup> [24]. However, in all of these works, S-doped TiO<sub>2</sub> electrodes were fabricated at elevated temperatures to guarantee the penetration of the S-dopants into the TiO<sub>2</sub> network. There are certain disadvantages associated with employing a high temperature route for sulfur doping. It may affect the tubular morphology and decrease the surface area. Moreover, it has been reported that the as-prepared TiO<sub>2</sub> nanotubes in an amorphous state provide higher specific capacities [25] and better rate capability [26] than crystalline TiO<sub>2</sub> due to a higher Li-ion diffusivity [7,27], while a high temperature processing step would lead to crystallization and may neutralize the doping advantage. Since high temperature routes also generally involve higher costs, facile synthesis of S-doped TiO<sub>2</sub> at lower temperatures is therefore highly desirable. Masahashi's group reported about visible light activity of sulfur-doped TiO<sub>2</sub> photo-electrodes, which were prepared by a single-step electrochemical anodization in aqueous sulfuric acid as electrolyte [28]. Although they showed that the doped sulfur ions with single step anodization could effectively narrow the TiO<sub>2</sub> band gap, non-self-organized TiO<sub>2</sub> layers were fabricated. The self-organized porous amorphous TiO<sub>2</sub> structure has a larger potential in view of rechargeable ion batteries [29], and hence the electrochemical anodization approach for S-doping needs to be established.

Herein, we report a direct method to prepare S-doped TiO<sub>2</sub> nanotubes using anodic oxidation. Modification of the organic electrolyte enabled in situ S-doping during anodization without the need for any additional processing. The S-doped TiO<sub>2</sub> anodes showed higher areal capacities as well as improved rate capability in comparison to undoped TiO<sub>2</sub> anodes. Thus, we present a promising approach for facile and cost-effective S-doping of mesoporous TiO<sub>2</sub> anodes with enhanced morphology towards an improved electrochemical performance in LIBs.

## 2. Results and Discussion

### 2.1. Preparation and Characterization of TiO<sub>2</sub> Nanotubes

Pure TiO<sub>2</sub> nanotubes and S-doped TiO<sub>2</sub> nanotubes (henceforth referred to as TNT and STNT, respectively) were obtained by anodic oxidation of titanium substrates. S-doping was done in situ during the anodization with addition of Na<sub>2</sub>S<sub>2</sub>O<sub>5</sub> in the electrolyte as the sulfur source. Figure 1 shows current density–time (I–t) curves during the anodization process. For a single-step anodization process, the I–t curve can be separated into three stages [30]. In Stage I, the current density drops almost exponentially due to a passivation effect from the formed oxide film. In the next stage, local

surface activation and pore formation takes place [7]. The establishment of steady state conditions leading to self-organized structure growth marks the beginning of Stage III, whence the I–t curve remains more or less constant. The profiles for the TNT and STNT samples are significantly different. The addition of  $\text{Na}_2\text{S}_2\text{O}_5$  affects the passivation and pore formation processes. Due to the S-species in STNT synthesis, the ionic transport during anodization is likely affected, decreasing the overall current density such that the I–t curve is located below that of the TNT sample [31].

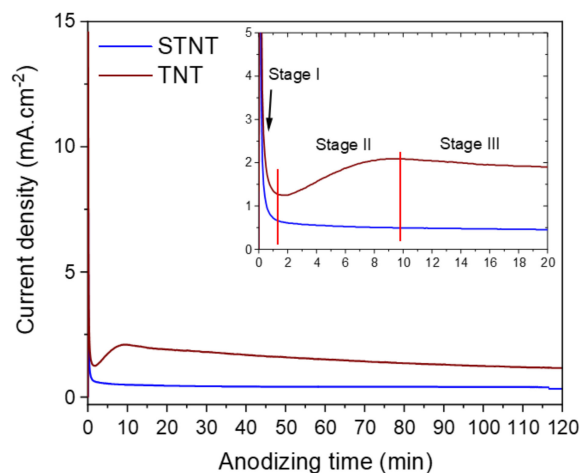


**Figure 1.** Time-current density plots during anodization for TNT and STNT samples. The inset shows the zoomed-in region around stage II.

A typical XRD pattern of as-prepared  $\text{TiO}_2$  nanotubes with and without S-doping confirms an amorphous character of the crystal structure (Figure S1 of supporting information). The amorphous phase is typical for  $\text{TiO}_2$  samples synthesized via an anodization process and further annealing  $280\text{ }^\circ\text{C}$  is commonly done in literature in order to obtain crystalline anatase or rutile phase [7].

The morphology of the as-prepared nanotube structures was characterized by scanning electron microscopy (SEM), and representative images of the top view of the TNT and STNT samples are shown in Figure 2. Both samples exhibit a highly ordered tubular structure. The TNT sample shows a uniform tube diameter of 60–70 nm, whereas a larger tube diameter of 140–160 nm was observed for the STNT sample. Energy-dispersive X-ray spectroscopy (EDS) measurements were also performed on the STNT samples and the data are given in Figure S2 of the supplement. The presence of S-doping was observed. Therefore, with  $\text{Na}_2\text{S}_2\text{O}_5$  addition to the electrolyte, not only could S-doping be realized, but it could also improve the morphology towards electrochemical processes as a larger pore diameter should facilitate ion transport inside the tubes.

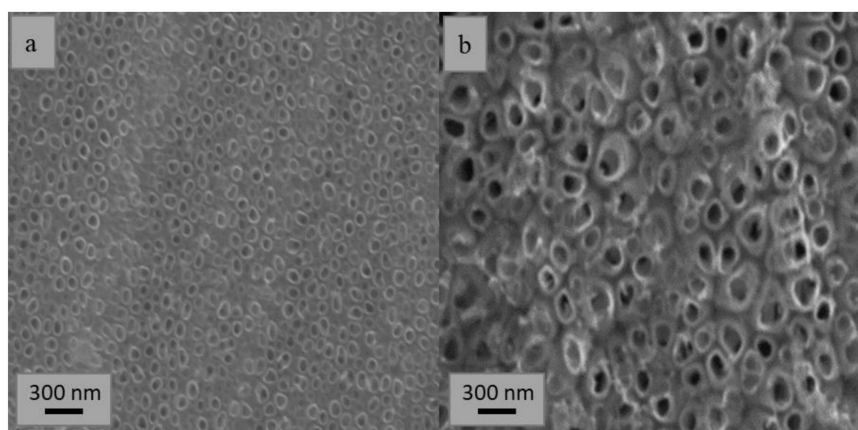


**Figure 2.** SEM images of the top-view of the samples prepared by anodic oxidation (a) TNT; (b) STNT.

In order to detect the S-content accurately, X-ray photoelectron spectroscopy (XPS) was carried out on the STNT sample; the elemental spectra are shown in Figure 3. As shown in Figure 3a, the Ti  $2p_{3/2}$  and Ti  $2p_{1/2}$  peaks for STNT are located at 459.25 and 465.00 eV, respectively, which fit well with  $\text{TiO}_2$ , as reported earlier [8,12]. The presence of S-doping, at least at the surface, is confirmed. The elemental percentage of S was found to be  $\sim 1.5$  at.%. Both the O 1s and S 2p spectra were fitted as well, and contributions from S-species were indexed. The O 1s peaks are located at 530.6, and 532.15 eV, which can be assigned to S-O-Ti, and S-O bonds, respectively [32] (Figure 3b). In the S 2p spectrum, the  $\text{S}^{2-}$  species (161.7 and 164.0 eV) and the  $\text{S}^{6+}$  species (168.8 eV), corresponding to the S-Ti, S-Ti-O and sulfate bonds, respectively [32] (Figure 3c), are assigned. To evaluate the presence of sulfur in the bulk, sputtering was done for 30 min ( $\sim 2.5 \text{ nm}\cdot\text{min}^{-1}$  based on silica standard). S is present in the material after sputtering as well (shown in the S 2p spectrum in Figure S3). Although the substitution of O with S at equilibrium states is unfavorable [33], the S doping is feasible with the anodization method.

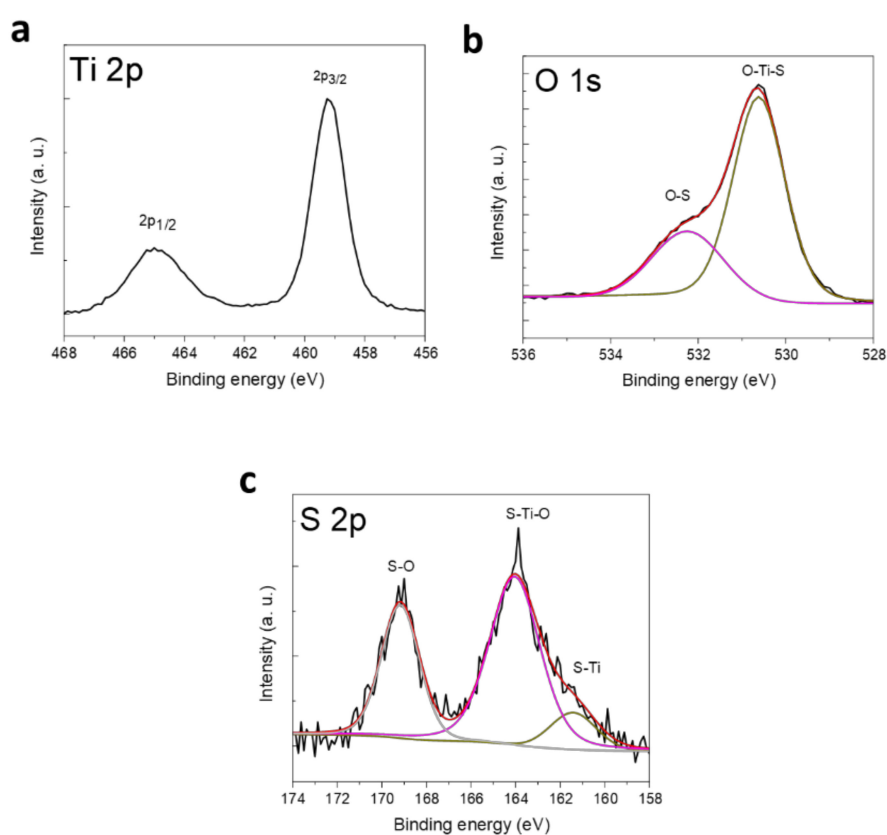


**Figure 3.** XP spectra for STNT samples (a) Ti 2p; (b) O 1s (c) S 2p. The black line corresponds to the measured spectra, the pink and yellow lines represent fitted data for each species, while the red line represents the whole calculated spectrum for O 1s and S 2p.

## 2.2. Electrochemical Properties of TNT and STNT

The electrochemical performance of the STNT samples was investigated in half-cells vs.  $\text{Li/Li}^+$ , along with TNT samples as baseline for comparison. The as-prepared nanotube samples were directly tested without annealing since previous reports have shown that amorphous  $\text{TiO}_2$  performs better than crystalline  $\text{TiO}_2$ , which is attributed to a more disordered structure [7,24–26].

Cycling voltammetry (CV) was performed on both samples for multiple cycles and the voltammograms for the 1st and 5th cycles are shown in Figure 4 (all the cycles are given in Figure S4 of the supplement). The CV behavior of the TNT sample is quite similar to that of amorphous  $\text{TiO}_2$  nanotube electrodes, as reported previously for the pure and mixed oxide system [34,35]. A pair of broad, symmetric peaks are observed corresponding to Li-ion insertion and extraction in the amorphous

material. For the STNT sample, the 1st cycle CV curve is noticeably different, likely due to the presence of a surface-layer with a higher sulfur content. In the 5th cycle, the CV curve is rather similar to the TNT sample (Figure 4b) although the reduction/oxidation peaks are even broader. Moreover, the area under the curve is higher than that of the TNT anode, indicating a higher energy density, and is therefore expected to show improved electrochemical performance.

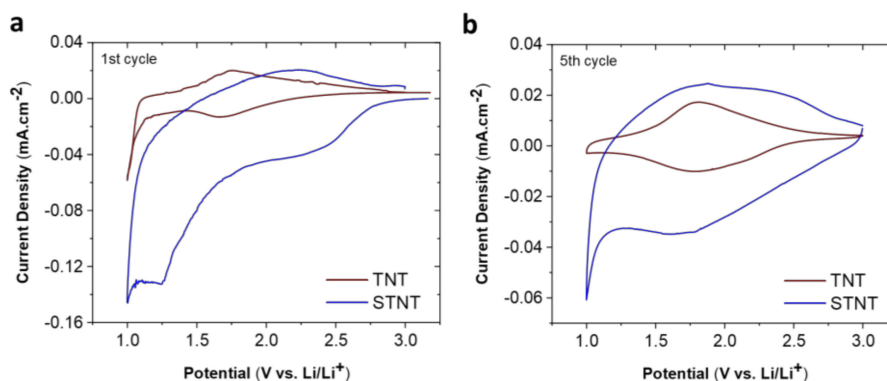


**Figure 4.** Cyclic voltammograms of TNT and STNT samples (a) 1st cycle; (b) 5th cycle.

Galvanostatic cycling was evaluated subsequently for both the samples. The voltage profile curves of the STNT and TNT materials during the 1st, 2nd, 5th, and 10th cycles, which are performed at a voltage range of 2.5–1 V vs. Li<sup>+</sup>/Li, are depicted in Figure 5a,b. The intercalation/de-intercalation plateaus are rather similar, suggesting that the electrochemical behavior is comparable. The discharge and charge capacities of STNT at a current density of 100  $\mu\text{A}\cdot\text{cm}^{-2}$  are 110 and 80  $\mu\text{Ah}\cdot\text{cm}^{-2}$  in the first cycle, much higher than the initial discharge/charge capacities of the TNT sample (63 and 53  $\mu\text{Ah}\cdot\text{cm}^{-2}$ , respectively). This irreversible capacity loss in the first cycle in both samples may be attributed to the reaction of some functional groups and species on the surface of titanium oxide with the electrolyte, which gives rise to decomposition of the electrolyte [8,15].

A similar improvement in the performance for the STNT anode is observed in the rate capability cycling shown in Figure 5c. The STNT anode shows areal capacities of 96, 58, 57, and 55  $\mu\text{Ah}\cdot\text{cm}^{-2}$  at 100, 250, 500, and 2500  $\mu\text{A}\cdot\text{cm}^{-2}$ , respectively, significantly higher than those obtained for the TNT anode at all current densities. When the current rate was reduced back to 100  $\mu\text{A}\cdot\text{cm}^{-2}$ , the STNT anode exhibits a stable capacity of 95  $\mu\text{Ah}\cdot\text{cm}^{-2}$ , suggesting excellent reversibility. The subsequent long-term cycling is shown in Figure 5d. Both STNT and TNT anodes show excellent cycling stability and demonstrated 95 and 56  $\mu\text{Ah}\cdot\text{cm}^{-2}$  areal capacity, respectively, at the end of 150 cycles, with STNT showing a higher average coulombic efficiency. Note that there is a small amount of irreversible capacity during the discharge process, likely due to side reactions from the electrolyte, leading to the Coulombic efficiency less than 100%. Such obtained results are comparable with previous reports that include multiple preparation steps such as SnO<sub>2</sub>@TiO<sub>2</sub> NT [36] and MoO<sub>3</sub>-deposited TiO<sub>2</sub> [37] electrodes, which showed average capacities of 113 and 116  $\mu\text{Ah}\cdot\text{cm}^{-2}$ , respectively, after only 50 cycles at current densities of 100 and 50  $\mu\text{A}\cdot\text{cm}^{-2}$ . Furthermore, STNT demonstrates higher areal capacity and rate performance than N-doped-TiO<sub>2</sub> NTs tested under the same current rates [38].

Electrochemical impedance spectroscopy (EIS) has also been applied to further understand the improvement in the performance. The charged-state Nyquist plots of the TNT and STNT materials are presented in Figure 6. For both samples, a well-defined semicircle at high frequencies was observed, corresponding to the charge transfer resistance of Li ions within hosts [35,39]. The EIS results were fitted with an equivalent circuit (shown in the inset of Figure 6), and STNT has a lower charge transfer resistance ( $31 \pm 3 \Omega$ ) compared to the TNT anode ( $92 \pm 2 \Omega$ ). Similar reduction in the charge transfer resistance was noticed after doping anatase nanoparticles prepared by hydrothermal reaction [23]. S-doping therefore improves the charge transfer in amorphous TiO<sub>2</sub> which, in conjunction with a larger pore diameter, enhances the electrochemical performance, particularly at high rates.

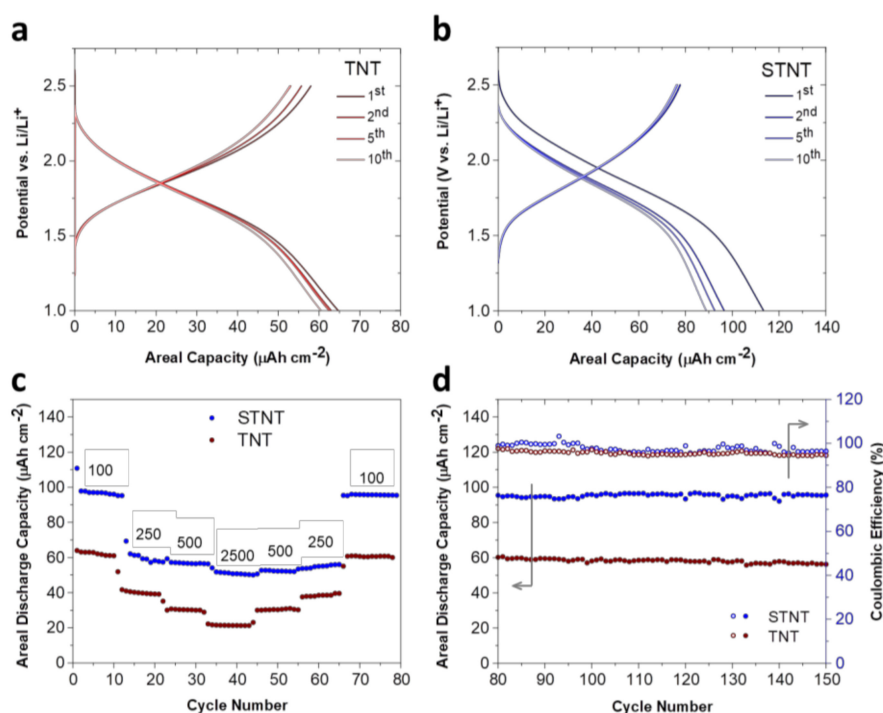


**Figure 5.** Galvanostatic voltage profiles at 100  $\mu\text{A}\cdot\text{cm}^{-2}$  for (a) TNT sample; (b) STNT sample, along with electrochemical performance; (c) rate capability for TNT and STNT samples showing areal discharge capacities; current rates are mentioned above the corresponding cycles in the unit of  $\mu\text{A}\cdot\text{cm}^{-2}$ ; and (d) subsequent long-term cycling for TNT and STNT anodes; corresponding y-axes are marked with arrows.

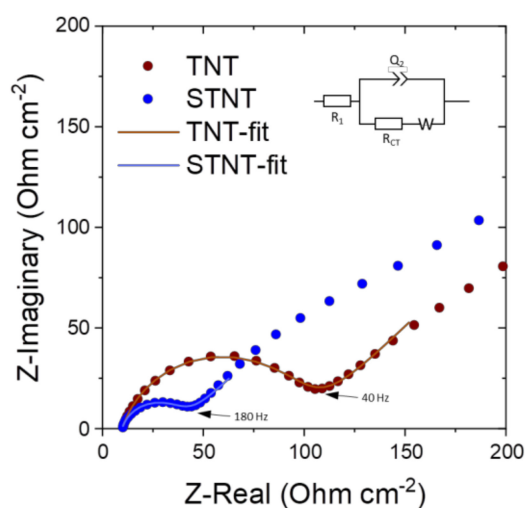


**Figure 6.** Nyquist Plots of STNT and TNT anodes along with the fits based on an equivalent circuit (shown in the inset).

In order to further explore the influence of the  $\text{Na}_2\text{S}_2\text{O}_5$  concentration on the morphology and electrochemical performance, anodization was carried out with a lower (0.045 M) and a higher concentration (0.135 M) of  $\text{Na}_2\text{S}_2\text{O}_5$  as compared to 0.09 M in the samples described above. Figure S5 in the supplement shows the time–current density plots for the anodization process. The anodization for 0.045 M concentration is quite similar to that of the TNT sample, whereas the 0.135 M concentration is similar to the STNT sample. Accordingly, the morphology of the sample prepared with 0.045 M concentration is quite similar to the TNT sample (Figure 7a); however, for 0.135 M concentration,

only a porous  $\text{TiO}_2$  structure with irregular pores is observed instead of self-organized nanotubes (Figure 7b). Rate capability tests were done to evaluate the change in electrochemical performance, and are shown in Figure 7c, along with the data for TNT and STNT for comparison. The areal capacities obtained for 0.045 M samples at different rates are almost exactly the same as that for the TNT sample, suggesting that the S-doping is negligible with a small concentration of  $\text{Na}_2\text{S}_2\text{O}_5$  and, therefore, does not lead to any noticeable change in the performance. In contrast, the rate capability of the 0.135 M sample is even lower than that of TNT, likely due to the absence of a uniform nanotubular structure, which is unfavorable for the lithiation/de-lithiation process. Thus, the 0.09 M  $\text{Na}_2\text{S}_2\text{O}_5$  concentration leads to better results since it not only enables S-doping, but also leads to advantageous morphological changes, while maintaining the self-organized nanotubular structure.

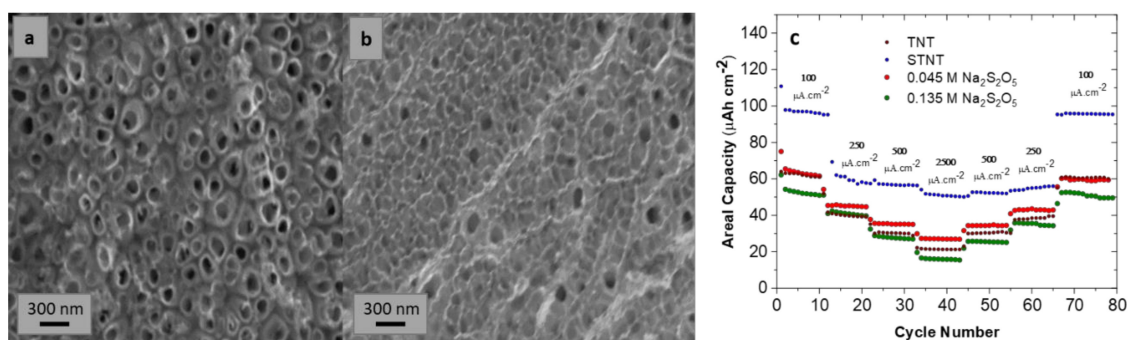


**Figure 7.** SEM images of the top-view of the samples prepared by anodic oxidation with (a) 0.045 M  $\text{Na}_2\text{S}_2\text{O}_5$ ; (b) 0.135 M  $\text{Na}_2\text{S}_2\text{O}_5$ , along with (c) rate capability data of the prepared electrodes in comparison to TNT and STNT samples.

### 3. Materials and Methods

#### 3.1. Fabrication of Pure $\text{TiO}_2$ Nanotubes and S-Doped $\text{TiO}_2$ Nanotubes

Pure  $\text{TiO}_2$  nanotubes were fabricated by a typical anodic oxidation process described elsewhere in detail [8]. Samples were prepared using an ethylene glycol/water solution (5% *v/v*) containing 0.09 M  $\text{NH}_4\text{F}$  (99% purity, Merck, Darmstadt, Germany) as electrolyte. The anodization process was carried out at room temperature in two electrode Teflon cells where a 12 mm diameter titanium substrate (99.5% purity, 0.25 mm thickness, Alfa Aesar, Karlsruhe, Germany) was utilized as the working electrode and platinum as the counter electrode, with a 2 cm distance between the electrodes. A voltage of 40 V was applied for 2 h at a rate of  $20 \text{ mV}\cdot\text{s}^{-1}$  using a programmable DC-power supply (Keithley 2400 source master). After anodization, samples were washed with deionized water to remove the residual debris. S-doped  $\text{TiO}_2$  nanotube samples were prepared using the same anodization process. For the sulfur source, sodium pyrosulfite ( $\text{Na}_2\text{S}_2\text{O}_5$ , analytical grade, Union Chimique Belge) was added to the electrolyte. Different samples were prepared with varying concentrations of  $\text{Na}_2\text{S}_2\text{O}_5$  (0.045 M, 0.09 M, and 0.135 M).

#### 3.2. Characterization

Scanning electron microscopy (SEM) was performed using a Gemini LEO 1530 (Zeiss, Oberkochen, Germany) field-emission scanning electron microscope. Energy-dispersive X-ray spectroscopy (EDXS) was done using a Bruker XFlash 4010 detector equipped with the QUANTAX software. X-ray photoelectron spectroscopy (XPS) measurements were carried out at a Physical Electronics PHI 5600 CI system using a hemispherical analyzer at a pass energy of 29 eV and a step size of 0.1 eV and with monochromatic Al  $\text{K}\alpha$  radiation (350 W) for excitation. The binding energy scale of the spectrometer was calibrated with metal foils of Au for the binding energy (BE) of Au  $4f_{7/2}$  at 84.0 eV and Cu foil for the BE of Cu  $2p_{3/2}$  at 932.7 eV. The binding energies of the spectra were calibrated according to

C 1s (284.8 eV). Elemental concentrations from the XPS were calculated using standard single-element sensitivity factors. The core level signals were fitted with a Gaussian function using a nonlinear Shirley-type background. Amorphous state of TiO<sub>2</sub> nanotubes, prepared at room temperature without and with S-doping, was confirmed by X-ray powder diffraction (STOE Stadi P, Co-K<sub>α</sub> radiation, Dectris Mythen 1K detector).

### 3.3. Electrochemical Testing

The electrochemical testing was done in Swagelok-type cells in the half-cell configuration. The as-prepared samples were utilized as working electrodes without additional binder or conductive additives. A pure lithium film (99.9%, Alfa Aesar) served as the counter electrode, and two pieces of glass fiber separator (Whatman, GF/D) were used. The electrolyte was LP30 (1 M LiPF<sub>6</sub>, in a 1:1 (v/v) mixture of ethylene carbonate and dimethyl carbonate, battery grade, BASF). The cells were assembled inside an argon filled glove box with water and oxygen content less than 0.1 ppm. Cyclic voltammetry, galvanostatic cycling, and electrochemical impedance spectroscopy (EIS) were conducted on a multichannel potentiostat (VMP3, Bio-Logic, Seyssinet-Pariset, France). Cyclic voltammetry tests were carried out between 1 and 3 V versus Li/Li<sup>+</sup> at a scan rate of 0.1 mV·s<sup>-1</sup>. The areal capacity is defined as total discharge/charge capacity per unit area of the electrode. The Coulombic efficiency was calculated as a percentage of Q<sub>charge</sub>/Q<sub>discharge</sub> as it is common for Li-free anode materials being tested in half-cells. The galvanostatic cycling was carried out within the voltage range of 1 and 3 V vs. Li/Li<sup>+</sup>. EIS measurements were performed in a frequency range of 0.01 Hz–100 kHz at a potential of 1.7 V with a perturbation signal of 5 mV. All electrochemical measurements were performed at 25 °C in controlled climate chambers.

## 4. Conclusions

We hereby successfully demonstrated direct S-doping of TiO<sub>2</sub> during the anodization process by addition of Na<sub>2</sub>S<sub>2</sub>O<sub>5</sub>. XPS studies confirmed the presence of differently charged sulfur species, which resulted in an improved conductivity of the TiO<sub>2</sub> framework. Moreover, the concentration of S-species in the electrolyte affected the morphology of the nanotubes. As a result, in combination with changes in morphology, the areal capacity was significantly improved (95 μAh·cm<sup>-2</sup> after 80 cycles versus 56 μAh·cm<sup>-2</sup> for pure TiO<sub>2</sub>), along with an enhanced rate capability in LIBs (demonstrating more than twice the specific capacity of pure TiO<sub>2</sub> at 2500 μAh·cm<sup>-2</sup>), thereby making the approach promising for practical implementation. Furthermore, beyond a certain Na<sub>2</sub>S<sub>2</sub>O<sub>5</sub> concentration in the electrolyte, porous, non-tubular morphology was observed for TiO<sub>2</sub> which deteriorated the electrochemical performance.

**Supplementary Materials:** The following are available online at <http://www.mdpi.com/2313-0105/6/4/51/s1>. Figure S1: Typical X-ray diffraction patterns of as-anodized Ti substrate with and without S-doping, Figure S2: EDXS measurements for the STNT samples showing clear signal for sulfur, Figure S3: S 2p spectrum for STNT sample after sputtering for 30 min, Figure S4: Cyclic voltammograms of TNT and STNT samples, Figure S5: Time-current density plots during anodization for samples prepared with different concentration of Na<sub>2</sub>S<sub>2</sub>O<sub>5</sub> along with that of TNT and STNT samples.

**Author Contributions:** D.S.: preparation, investigations, data analysis, and writing of the original draft. M.M. (Mahmoud Madian): conceptualization, supervision, methodology, investigations, discussion review, and editing. A.O.: methodology, conceptualization, investigation, supervision, discussion, writing—review and editing. S.O.: investigation. M.U.: methodology, discussion. M.M. (Morteza Maghrebi): discussion, supervision. M.B.: discussion, supervision. D.M.: supervision, methodology, validation, writing—review and editing. All authors have read and agreed to the published version of the manuscript.

**Funding:** The work was supported by the European Union and the Free State of Saxony under the TTKin (SAB Grant No. 100225299), and Federal Ministry of Education and Research (BMBF) under Grant No. 03X4637 (WING-Center: Battery–Mobile in Saxony (BamoSa)).

**Acknowledgments:** We would like to acknowledge Steffi Kaschube (IFW Dresden) for assistance with XPS measurements.

**Conflicts of Interest:** There is no conflict of interest.



## References

1. Ould Amrouche, S.; Rekioua, D.; Rekioua, T.; Bacha, S. Overview of energy storage in renewable energy systems. *Int. J. Hydrog. Energy* **2016**, *41*, 20914–20927. [[CrossRef](#)]
2. González, A.; Goikolea, E.; Barrena, J.A.; Mysyk, R. Review on supercapacitors: Technologies and materials. *Renew. Sust. Energy Rev.* **2016**, *58*, 1189–1206. [[CrossRef](#)]
3. Nayak, P.K.; Erickson, E.M.; Schipper, F.; Penki, T.R.; Munichandraiah, N.; Adelhelm, P.; Sclar, H.; Amalraj, F.; Markovsky, B.; Aurbach, D. Review on challenges and recent advances in the electrochemical performance of high capacity Li- and Mn-rich cathode materials for Li-ion batteries. *Adv. Energy Mater.* **2018**, *8*, 1702397. [[CrossRef](#)]
4. Chen, C.; Hu, X.; Wang, Z.; Xiong, X.; Hu, P.; Liu, Y.; Huang, Y. Controllable growth of TiO<sub>2</sub>-B nanosheet arrays on carbon nanotubes as a high-rate anode material for lithium-ion batteries. *Carbon* **2014**, *69*, 302–310. [[CrossRef](#)]
5. Opra, D.P.; Gnedenkov, S.V.; Sinebryukhov, S.L.; Voit, E.I.; Sokolov, A.A.; Ustinov, A.Y.; Zheleznov, V.V. Zr<sup>4+</sup>/F-co-doped TiO<sub>2</sub> (anatase) as high performance anode material for lithium-ion battery. *Prog. Nat. Sci. Mater. Int.* **2018**, *28*, 542–547. [[CrossRef](#)]
6. Ming, H.; Li, X.; Su, L.; Liu, M.; Jin, L.; Bu, L.; Kang, Z.; Zheng, J. One step synthesis of C&N co-doped mesoporous TiO<sub>2</sub> with enhanced performance in a lithium-ion battery. *RSC Adv.* **2013**, *3*, 3836–3839.
7. Madian, M.; Eychmüller, A.; Giebel, L. Current advances in TiO<sub>2</sub>-based nanostructure electrodes for high performance lithium ion batteries. *Batteries* **2018**, *4*, 7. [[CrossRef](#)]
8. Madian, M.; Klose, M.; Jaumann, T.; Gebert, A.; Oswald, S.; Ismail, N.; Eychmüller, A.; Eckert, J.; Giebel, L. Anodically fabricated TiO<sub>2</sub>-SnO<sub>2</sub> nanotubes and their application in lithium ion batteries. *J. Mater. Chem. A* **2016**, *4*, 5542–5552. [[CrossRef](#)]
9. Zhu, G.N.; Wang, Y.G.; Xia, Y.Y. Ti-based compounds as anode materials for Li-ion batteries. *Energy Environ. Sci.* **2012**, *5*, 6652–6667. [[CrossRef](#)]
10. Feckl, J.M.; Fominykh, K.; Döblinger, M.; Fattakhova-Rohlfing, D.; Bein, T. Nanoscale porous framework of lithium titanate for ultrafast lithium insertion. *Angew. Chem. Int. Ed. Engl.* **2012**, *51*, 7459–7463. [[CrossRef](#)]
11. Li, J.; Zhang, X.; Han, L.; Yan, D.; Hou, S.; Lu, T.; Yao, Y.; Pan, L. TiO<sub>2</sub> nanocrystals embedded in sulfur-doped porous carbon as high-performance and long-lasting anode materials for sodium-ion batteries. *J. Mater. Chem. A* **2018**, *6*, 24224–24231. [[CrossRef](#)]
12. Liu, J.; Song, K.; van Aken, P.A.; Maier, J.; Yu, Y. Self-supported Li<sub>4</sub>Ti<sub>5</sub>O<sub>12</sub>-C nanotube arrays as high-rate and long-life anode materials for flexible Li-ion batteries. *Nano Lett.* **2014**, *14*, 2597–2603. [[CrossRef](#)]
13. Oh, Y.; Nam, S.; Wi, S.; Kang, J.; Hwang, T.; Lee, S.; Park, H.H.; Cabana, J.; Kim, C.; Park, B. Effective wrapping of graphene on individual Li<sub>4</sub>Ti<sub>5</sub>O<sub>12</sub> grains for high-rate Li-ion batteries. *J. Mater. Chem. A* **2014**, *2*, 2023–2027. [[CrossRef](#)]
14. Reddy, M.V.; Sharma, N.; Adams, S.; Rao, R.P.; Peterson, V.K.; Chowdari, B.V.R. Evaluation of undoped and M-doped TiO<sub>2</sub>, where M = Sn, Fe, Ni/Nb, Zr, V, and Mn, for lithium-ion battery applications prepared by the molten-salt method. *RSC Adv.* **2015**, *5*, 29535–29544. [[CrossRef](#)]
15. Lan, T.; Zhang, W.; Wu, N.L.; Wei, M. Nb-Doped rutile TiO<sub>2</sub> mesocrystals with enhanced lithium storage properties for lithium ion battery. *Chem. Euro. J.* **2017**, *23*, 5059–5065. [[CrossRef](#)]
16. Cravanzola, S.; Cesano, F.; Gaziano, F.; Scarano, D. Sulfur-doped TiO<sub>2</sub>: Structure and surface properties. *Catalysts* **2017**, *7*, 214. [[CrossRef](#)]
17. Jiao, W.; Li, N.; Wang, L.; Wen, L.; Li, F.; Liu, G.; Cheng, H.-M. High-rate lithium storage of anatase TiO<sub>2</sub> crystals doped with both nitrogen and sulfur. *Chem. Commun.* **2013**, *49*, 3461–3463. [[CrossRef](#)]
18. Liu, S.; Cai, Z.; Zhou, J.; Pan, A.; Liang, S. Nitrogen-doped TiO<sub>2</sub> nanospheres for advanced sodium-ion battery and sodium-ion capacitor applications. *J. Mater. Chem. A* **2016**, *4*, 18278–18283. [[CrossRef](#)]
19. Jung, H.-G.; Yoon, C.S.; Prakash, J.; Sun, Y.-K. Mesoporous anatase TiO<sub>2</sub> with high surface area and controllable pore size by F<sup>-</sup> ion doping: Applications for high-power Li-ion battery anode. *J. Phys. Chem. C* **2009**, *113*, 21258–21263. [[CrossRef](#)]
20. Umebayashi, T.; Yamaki, T.; Itoh, H.; Asai, K. Band gap narrowing of titanium dioxide by sulfur doping. *Appl. Phys. Lett.* **2002**, *81*, 454–456. [[CrossRef](#)]
21. Tang, X.; Li, D. Sulfur-doped highly ordered TiO<sub>2</sub> nanotubular arrays with visible light response. *J. Phys. Chem. C* **2008**, *112*, 5405–5409. [[CrossRef](#)]

22. Ksibi, M.; Rossignol, S.; Tatibouët, J.-M.; Trapalis, C. Synthesis and solid characterization of nitrogen and sulfur-doped TiO<sub>2</sub> photocatalysts active under near visible light. *Mater. Lett.* **2008**, *62*, 4204–4206. [[CrossRef](#)]
23. Li, F.; Liu, W.; Lai, Y.; Qin, F.; Zou, L.; Zhang, K.; Li, J. Nitrogen and sulfur co-doped hollow carbon nanofibers decorated with sulfur doped anatase TiO<sub>2</sub> with superior sodium and lithium storage properties. *J. Alloys. Compd.* **2017**, *695*, 1743–1752. [[CrossRef](#)]
24. Ni, J.; Fu, S.; Wu, C.; Maier, J.; Yu, Y.; Li, L. Self-supported nanotube arrays of Sulfur-doped TiO<sub>2</sub> enabling ultrastable and robust Sodium storage. *Adv. Mater.* **2016**, *28*, 2259–2265. [[CrossRef](#)]
25. Guan, D.; Cai, C.; Wang, Y. Amorphous and crystalline TiO<sub>2</sub> nanotube arrays for enhanced Li-ion intercalation properties. *J. Nanosci. Nanotech.* **2011**, *11*, 3641–3650. [[CrossRef](#)]
26. Fang, H.T.; Liu, M.; Wang, D.W.; Sun, T.; Guan, D.S.; Li, F.; Zhou, J.; Sham, T.K.; Cheng, H.M. Comparison of the rate capability of nanostructured amorphous and anatase TiO<sub>2</sub> for lithium insertion using anodic TiO<sub>2</sub> nanotube arrays. *Nanotechnology* **2009**, *20*, 225701. [[CrossRef](#)]
27. Ryu, W.H.; Nam, D.H.; Ko, Y.S.; Kim, R.H.; Kwon, H.S. Electrochemical performance of a smooth and highly ordered TiO<sub>2</sub> nanotube electrode for Li-ion batteries. *Electrochim. Acta* **2012**, *61*, 19–24. [[CrossRef](#)]
28. Mizukoshi, Y.; Ohtsu, N.; Semboshi, S.; Masahashi, N. Visible light responses of sulfur-doped rutile titanium dioxide photocatalysts fabricated by anodic oxidation. *Appl. Catal. B Environ.* **2009**, *91*, 152–156. [[CrossRef](#)]
29. Indira, K.; Mudali, U.K.; Nishimura, T.; Rajendran, N. A review on TiO<sub>2</sub> nanotubes: Influence of anodization parameters, formation mechanism, properties, corrosion behavior, and biomedical applications. *J. Bio. Tribo-Corros.* **2015**, *1*, 28. [[CrossRef](#)]
30. Macak, J.M.; Tsuchiya, H.; Ghicov, A.; Yasuda, K.; Hahn, R.; Bauer, S.; Schmuki, P. TiO<sub>2</sub> nanotubes: Self-organized electrochemical formation, properties and applications. *Curr. Opin. Solid State Mater. Sci.* **2007**, *11*, 3–18. [[CrossRef](#)]
31. Mazierski, P.; Nischk, M.; Gołkowska, M.; Lisowski, W.; Gazda, M.; Winiarski, M.J.; Klimczuk, T.; Zaleska-Medynska, A. Photocatalytic activity of nitrogen doped TiO<sub>2</sub> nanotubes prepared by anodic oxidation: The effect of applied voltage, anodization time and amount of nitrogen dopant. *Appl. Catal. B Environ.* **2016**, *196*, 77–88. [[CrossRef](#)]
32. Moulder, J.F.; Stickle, W.F.; Sobol, P.E.; Bomben, K.D. *Handbook of X-Ray Photoelectron Spectroscopy*; Chastain, J. Ed.; Perkin-Elmer Corporation: Eden Prairie, MI, USA, 1992; p. 261.
33. Asahi, R.; Morikawa, T.; Ohwaki, T.; Aoki, K.; Taga, Y. Visible-light photocatalysis in nitrogen-doped titanium oxides. *Science* **2001**, *293*, 269–271. [[CrossRef](#)] [[PubMed](#)]
34. Madian, M.; Ummethala, R.; Abo El Naga, A.O.; Ismail, N.; Rummeli, M.H.; Eychmüller, A.; Giebeler, L. Ternary CNTs@TiO<sub>2</sub>/CoO nanotube composites: Improved anode materials for high performance lithium ion batteries. *Materials* **2017**, *10*, 678. [[CrossRef](#)] [[PubMed](#)]
35. Madian, M.; Wang, Z.; Gonzalez-Martinez, I.; Oswald, S.; Giebeler, L.; Mikhailova, D. Ordered Ti-Fe-O nanotubes as additive-free anodes for lithium ion batteries. *Appl. Mater. Today* **2020**, *20*, 100676. [[CrossRef](#)]
36. Wu, X.; Zhang, S.; Wang, L.; Du, Z.; Fang, H.; Ling, Y.; Huang, Z. Coaxial SnO<sub>2</sub>@TiO<sub>2</sub> nanotube hybrids: From robust assembly strategies to potential application in Li<sup>+</sup> storage. *J. Mater. Chem.* **2012**, *22*, 11151. [[CrossRef](#)]
37. Guan, D.; Li, J.; Gao, X.; Yuan, C. Controllable synthesis of MoO<sub>3</sub>-deposited TiO<sub>2</sub> nanotubes with enhanced lithium-ion intercalation performance. *J. Power Sources* **2014**, *246*, 305–312. [[CrossRef](#)]
38. Appadurai, T.; Subramaniam, C.M.; Kuppusamy, R.; Karazhanov, S.; Subramanian, B. Electrochemical Performance of Nitrogen-Doped TiO<sub>2</sub> Nanotubes as Electrode Material for Supercapacitor and Li-Ion Battery. *Molecules* **2019**, *24*, 2952. [[CrossRef](#)] [[PubMed](#)]
39. Madian, M.; Giebeler, L.; Klose, M.; Jaumann, T.; Uhlemann, M.; Gebert, A.; Oswald, S.; Ismail, N.; Eychmüller, A.; Eckert, J. Self-organized TiO<sub>2</sub>/CoO nanotubes as potential anode materials for lithium ion batteries. *ACS Sustain. Chem. Eng.* **2015**, *3*, 909–919. [[CrossRef](#)]

**Publisher’s Note:** MDPI stays neutral with regard to jurisdictional claims in published maps and institutional affiliations.



© 2020 by the authors. Licensee MDPI, Basel, Switzerland. This article is an open access article distributed under the terms and conditions of the Creative Commons Attribution (CC BY) license (<http://creativecommons.org/licenses/by/4.0/>).